Journal of Power Sources 243 (2013) 481–487

Contents lists available at SciVerse ScienceDirect

Journal of Power Sources

journal homepage: www.elsevier.com/locate/jpowsour

Novel rapid synthesis method of $LiFePO_4$/C cathode material by high-frequency induction heating

Satoshi Uchida, Masaki Yamagata, Masashi Ishikawa*

Department of Chemistry and Materials Engineering, Faculty of Chemistry, Materials and Bioengineering, Kansai University, 3-3-35 Yamate-cho, Suita 564-8680, Japan

HIGHLIGHTS

- A novel low-cost synthesis of a $LiFePO_4$/carbon composite cathode is proposed.
- This combines high-frequency induction heating with carbothermal reduction.
- Our method uses a very inexpensive Fe_2O_3 as a Fe source.
- The $LiFePO_4$ composite is synthesized within a few minutes at 900 °C.

ARTICLE INFO

Article history:
Received 12 May 2013
Received in revised form
6 June 2013
Accepted 7 June 2013
Available online 14 June 2013

Keywords:
Induction heating
Carbothermal reduction
$LiFePO_4$
Li-ion battery

ABSTRACT

We propose a novel low-cost synthesis method of a $LiFePO_4$/C composite with excellent battery performances that combine high-frequency induction heating with carbothermal reduction. Our method uses a very inexpensive Fe_2O_3 as a Fe source. The $LiFePO_4$/C is synthesized in far less time (within a few minutes) at 900 °C than in a conventional method. Although the initially synthesized $LiFePO_4$/C (LFP-120) contains such over-reduction impurities as Fe_2P or Fe_3P, optimized $LiFePO_4$/C (LFP-90) containing no impurities is obtained by adjusting the heating time. Moreover, the primary particle size of the LFP-90 is sufficiently small to achieve fast Li-ion diffusion. The cathode containing LFP-90 has good charge–discharge rate performance and shows discharge capacities of 153.3 and 100.1 mAh g^{-1} at 1/10 and 10C-rates. The cathode with LFP-90 has excellent cycle stability and shows no degradation after high-rate charge–discharge tests. Our method reasonably reduces the manufacturing cost of $LiFePO_4$/C.

1. Introduction

Lithium iron phosphate ($LiFePO_4$), which has an olivine-type structure reported by Padhi et al. [1], is an attractive cathode material for Li-ion batteries due to such good electrochemical characteristics as flat potential around 3.5 V vs. Li/Li^+ for Li insertion/extraction and a theoretical capacity of 170 mAh g^{-1} with long cycle stability, high thermal stability, and low environmental impact. $LiFePO_4$ is also an excellent material from the viewpoint of an elemental strategy because it contains absolutely no rare metals [2]. Low electronic conductivity [3] and low Li-ion diffusivity [4], both of which cause low battery performances of $LiFePO_4$, have already been improved by modifying the surface of $LiFePO_4$ particles with carbon and decreasing the particle size [5–8]. The advantage of the $LiFePO_4$ cathode material described above may significantly reduce the costs and extend the cycle life of Li-ion batteries. Therefore, Li-ion batteries, including $LiFePO_4$ modified with carbon ($LiFePO_4$/C) [9,10] as a cathode, are especially suitable for such large scale applications as electric vehicles (EVs), hybrid electric vehicles (HEVs), and large storage systems for natural energy generation like wind or solar power.

To improve the battery performances of $LiFePO_4$/C cathode material, various synthesis methods have been reported. The following are all useful for the synthesis of $LiFePO_4$/C and provide excellent battery performances: a solid-state reaction [11], a polyol process [12], a sol–gel process [13,14], a hydrothermal method [15–17], a solvothermal method [18,19], splay pyrolysis [20,21], mechanical activation [22], and coprecipitation [23]. However, most of these methods use relatively expensive divalent iron compounds as iron sources and require a complex synthesis process or a long heating process of several hours to obtain a $LiFePO_4$ phase in an inert gas or a vacuum for suppressing the oxidation of

* Corresponding author.
E-mail address: masaishi@kansai-u.ac.jp (M. Ishikawa).

0378-7753/$ – see front matter © 2013 Elsevier B.V. All rights reserved.
http://dx.doi.org/10.1016/j.jpowsour.2013.06.040

iron (from Fe^{2+} to Fe^{3+}). As a result, $LiFePO_4$/C becomes expensive and has not been widely commercialized despite its excellent battery performances. Because such problems exist, few low-cost synthesis methods for $LiFePO_4$/C have been reported. Microwave synthesis is one low-cost method [24–26], but microwave controllability remains inadequate to obtain $LiFePO_4$/C with high battery performance. Thus, microwave synthesis is not applicable to mass production.

In this study, we propose a novel low-cost synthesis method to obtain $LiFePO_4$/C with high battery performances by combining high-frequency induction heating with carbothermal reduction [27]. Carbon sources are added beforehand to the precursor for carbothermal reduction as well as for the carbon modification of the $LiFePO_4$ surface. To reduce the heating period, we adopted high-frequency induction heating, which provides a very fast temperature rise to a desired temperature. Carbothermal reduction also allows the use of very inexpensive Fe_2O_3 as an iron source. The novel synthesis method proposed in this work reduces the manufacturing costs of $LiFePO_4$/C in terms of both process and material costs. The $LiFePO_4$/C composite is generated by the carbothermal reduction of Fe_2O_3. First, the carbon sources are thermally decomposed and carbonized. The resulting carbon deprives the Fe_2O_3 of its oxygen in a vacuum or an inert gas. Then a $LiFePO_4$ phase is generated from the divalent iron and other raw materials based on the following reaction [28]:

$$Li_2CO_3 + Fe_2O_3 + 2NH_4H_2PO_4 + 0.5C \rightarrow 2LiFePO_4 + 2NH_3 + 3H_2O + 1.5CO_2 .$$

The residual carbon, which is not consumed during the carbothermal reduction, remains on the surface of the $LiFePO_4$ particles and functions as a conductive agent.

2. Experimental

$LiFePO_4$/C samples were synthesized by a solid-state reaction of stoichiometric amounts of Li_2CO_3 (Kanto Chemical Co., 99.0%), Fe_2O_3 (Kishida Chemical Co., 98.5%), and $NH_4H_2PO_4$ (Kanto Chemical Co., 99.0%). The precursor was a mixture of the above materials with 10 wt.% citric acid (Kanto Chemical Co., 99.0%) or sucrose (Kanto Chemical Co., 99.0%) as a carbon source by planetary ball-milling for 5 h in an ethanol medium. The rotating speed was 400 rpm, and the ball-to-powder weight ratio was 20:1. After drying at 80 °C over 6 h in air to remove the ethanol, the obtained mixture was pressed into a 2–3 mm thick pellet at 21 MPa (30 kN). The pellet was set in a carbon crucible, which was placed in a vacuum chamber. The carbon crucible was rapidly heated to 700 or 900 °C at 1500–3000 °C min^{-1} by high-frequency induction heating and held for 1 h or 90–120 s at each maximum temperature in a vacuum. After the heating process, the carbon crucible was rapidly cooled to room temperature. The resulting gray or black pellets were ground thoroughly in a mortar, and the obtained power was used as a cathode active material.

We prepared the cathodes for the electrochemical performance tests in a dry room with a dew point of −55 °C. The synthesized cathode active materials were mixed with ketjen black (Lion Corp., Carbon ECP) and polyvinylidene fluoride (Kureha Corp., #1100) with a respective weight ratio of 85:8:7 in an adequate amount of *N*-methyl-2-pyrrolidone (Kishida Chemical Co., 99.5%) solvent. The obtained slurry was cast onto an Al-foil current collector and dried at 100 °C for 10 h in a vacuum oven. The prepared cathode sheets were cut into 12-mm diameter disks as a test cathode. The mass loading of the active material in the electrodes was 4.2–4.7 mg cm^{-2}.

Electrochemical measurements were carried out using a flat-type cell (Hosen Co.) assembled in an argon-filled globe box with the prepared test cathode, a Li foil (Honjo Metal Corp.) cut into 13-mm diameter disk as an anode, a 1 M $LiPF_6$ solution with an ethylene carbonate-dimethyl carbonate (1:1 v/v) (Kishida Chemical Co., LBG) as an electrolyte, and a polypropylene porous film as a separator. We carried out the charge–discharge measurement including cycle performance tests in a voltage range of 2.5–4.2 V on a galvanostatic charge–discharge unit (BTS2004W, Intex Co.). Rate performance tests were carried out at 1/10, 1/5, 1/2, 1, 3, 5, and 10C-rates (1C = 170 mA g^{-1}) in every 5th cycle. The stability against such various rate charging–discharging was assessed by a retest back to the initial 1/10C-rate after various rate tests. The cycle performances were evaluated for 50 cycles by galvanostatic charge–discharge at 1C-rate without any pre-cycles.

X-ray diffraction (XRD, Ultima IV, Rigaku Co.) with Cu Kα radiation was used to identify the phases of the synthesized samples. A graphite monochromator was used for the diffracted beams. The diffraction data were collected between 10 and 50° by a step scan mode with scanning steps of 0.02° and a sampling time of 5 s. The morphology of the secondary particles was observed using a scanning electron microscope (SEM, SU-1500, Hitachi Co.). The particle size of the synthesized samples was observed in the secondary electron (SE) images, and the compositional information was obtained from the back-scatter electron (BSE) images. We observed the morphology of the primary particles and the residual carbon on the surface of the particles using a transmission electron microscope (TEM, JEM-1400, JEOL Co.). The chemical state of the iron in the synthesized samples was analyzed by Mössbauer spectroscopy (measured by Toray Research Center Inc.) with ^{57}Co/Rh radiation, and the spectrometer worked in a constant acceleration mode. The transition between the ground state and the lowest excited state of ^{57}Fe was used for our analysis. The synthesized sample powder and a small amount of polyethylene powder were mixed and molded into tablets, which were sealed in an aluminum laminate pack in an argon-filled glove box to suppress the sample's oxidation during the measurement. The primary particle distribution of the synthesized samples was determined by small-angle X-ray scattering (SAXS, Ultima IV, Rigaku Co.); 30–70% of the direct beam was scattered by adjusting the thickness of the samples, and the scattering profiles were collected between 0.08 and 2.00°. The X-ray scattering derived from the air was deducted as background. The particle size distributions were determined by curve fitting to the scattering profiles using such parameters as background intensity, average particle size, normalized distribution ratio, scale factor, and the true density of $LiFePO_4$ (3.60 g cm^{-3}).

3. Results and discussion

Fig. 1 shows the XRD patterns of the synthesized samples sintered at 700 °C for 1 h with 10 wt.% citric acid (LFP-C) and 10 wt.% sucrose (LFP-S). The orthorhombic olivine phase (Space group: Pnma) which is shown as a reference pattern (JCPDS 80-2092) was observed in both samples, indicating that $LiFePO_4$/C was generated by high-frequency induction heating in far less time than a conventional method. However, LFP-C contains a slight impurity phase and LFP-S contains a large amount of impurities. These impurities are the Fe_2P and Fe_3P phases generated by over-reduction of the $LiFePO_4$ phase [29,30]. The presence of impurities in the synthesized samples implies the heterogeneous progress of the carbothermal reduction. The difference in the amount of impurities indicates that the homogeneity of the carbothermal reduction varies with the carbon sources. The citric acid soluble in ethanol was dispersed homogeneously in the overall precursor during ball-milling, and the sucrose insoluble in ethanol was present heterogeneously in the precursor. Therefore, the carbothermal reduction proceeds locally and a large amount of impurities are generated in

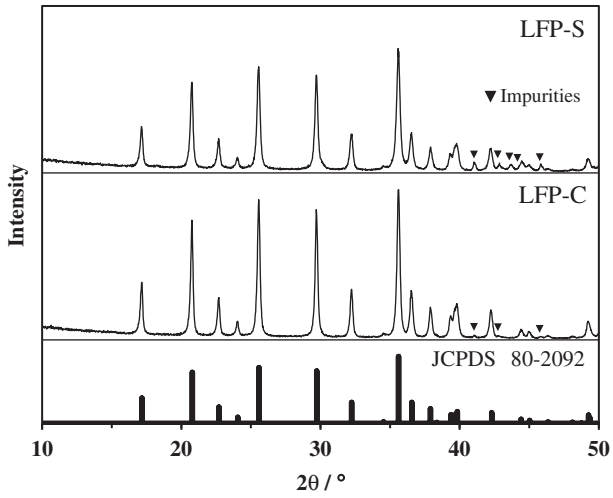

Fig. 1. XRD patterns of synthesized samples heated at 700 °C with sucrose (LFP-S) and citric acid (LFP-C) as carbon source. Reference pattern of $LiFePO_4$ phase (JCPDS 80-2092) is shown at the bottom.

LFP-S, whose peak intensity is much smaller than that of LFP-C. The generation of impurities due to inhomogeneous carbothermal reduction significantly reduces the amount of $LiFePO_4$ phase in LFP-S.

Fig. 2 shows the SEM images of LFP-S (a, b) and LFP-C (c, d). The secondary electron (SE) images (a) and (c) show the difference in particle size between LFP-C and LFP-S. The large particles observed in Fig. 2(a) are not aggregates because we carefully crushed the synthesized pellet samples in a mortar. In other words, the observed large particles are very hard, sintered particles that cannot be crushed any more. The LFP-C particles are much smaller than the LFP-S particles. Since the particle growth due to sintering is suppressed by the residual carbon, which is not consumed during the carbothermal reduction and prevents contact between $LiFePO_4$ particles, the distribution of the carbon source in the precursor is crucial. The inhomogeneous distribution of sucrose in the precursor is insufficient to suppress particle growth. The back-scattered electron (BSE) images (b) and (d) show the compositional information. The circled bright spots denote the concentration of relatively heavy elements; in this case, they should be agglomerates that contain Fe species and probably correspond to such crystalline impurity phases as Fe_2P or Fe_3P in the LFP-S confirmed in the XRD pattern. Judging from the preceding results, we believe that sucrose is inappropriate as a carbon source in our method. On the other hand, bright spots are only barely observed in Fig. 2(d), which indicates almost an absence of Fe_2P and Fe_3P phases in LFP-C. This is also in good agreement with the XRD results.

Fig. 3 shows the charge–discharge curves of the prepared cathodes containing LFP-C or LFP-S at a 1/10C-rate (1C = 170 mA g^{-1}). The voltage plateau around 3.5 V based on a Fe^{2+}/Fe^{3+} redox couple in the olivine structure was observed in both cathodes. The LFP-C and LFP-S cathodes show discharge capacities of 71.6 and 118.6 mAh g^{-1} in the initial cycle and exhibit stable discharge capacities in subsequent cycles. Although the Fe_2P and Fe_3P phases contained in each sample do not spoil the cycle performances, the generation of such impurities should not be ignored because a large amount of impurities is directly related to the loss of the $LiFePO_4$ portion and decreases the charge–discharge capacity of the synthesized samples. Even though LFP-C shows a larger charge–discharge capacity than LFP-S, it remains far from the theoretical capacity (170 mAh g^{-1}). LFP-C barely contains such crystalline impurities as Fe_2P and Fe_3P phases in the XRD and BSE observation results. However, XRD and BSE observation cannot essentially detect non-crystalline impurities and non-localized heavy elements. Thus, the present charge–discharge performance of LFP-C may be limited by other undetected impurities.

To find other causes for the limitation of the charge–discharge capacity of LFP-C, we investigated the chemical state of Fe in LFP-C. Fig. 4 shows the Mössbauer spectrum obtained from LFP-C. For the curve fitting results, the spectrum can be divided into three types of

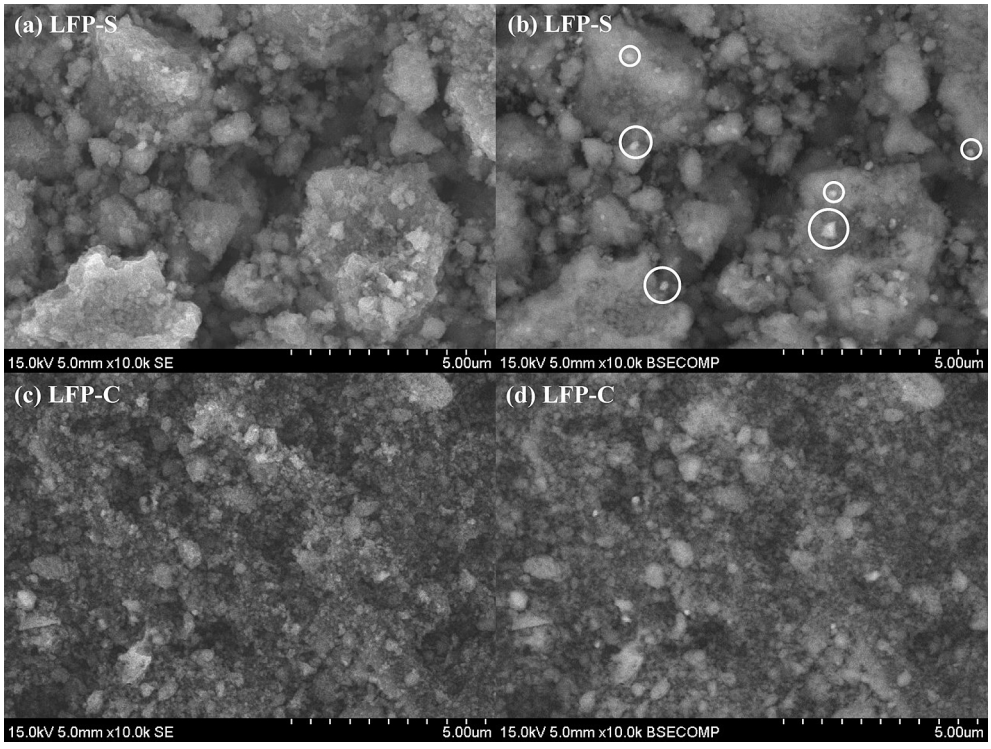

Fig. 2. SEM images: (a, b) LFP-S and (c, d) LFP-C. Left side shows SE images, and right side shows BSE images.

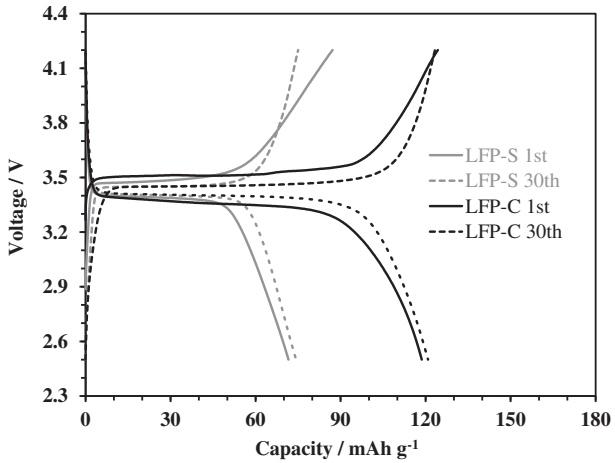

Fig. 3. Charge–discharge curves of cathodes containing LFP-S and LFP-C at 1/10C-rate (1C-rate = 170 mAh g^{-1}).

doublets. Table 1 summarizes the isomer shift, the quadrupole splitting, the abundance, and the chemical state of Fe corresponding to each doublet. The isomer shift and the quadrupole splitting for the strong doublet labeled State 1 can be attributed to typical divalent iron. The other doublets are attributed to Fe^{3+} labeled States 2 or 3. However, States 2 and 3 are close to the Fe^{2+} state because their isomer shifts are larger than that of typical Fe^{3+} (δ = 0.3 mm s^{-1}). Moreover, the quadrupole splitting of State 2 is much larger than that of typical Fe^{3+}, which indicates the low symmetry of its electron orbital. The 3d orbital of typical Fe^{3+} is a half-filled subshell with spherical symmetry. In other words, its lower symmetry denotes the existence of the sixth electron and suggests that State 2 is closer to the Fe^{2+} state than State 3. Based on the above interpretation, Fe labeled States 2 and 3 are derived from the raw material (Fe_2O_3) or its decomposition products. Since a slight over-reduction byproduct is confirmed in the XRD pattern for LFP-C, it does not contain much impurity. But actually, 2% Fe^{3+} labeled State 2 and 7% Fe^{3+} labeled State 3, derived from Fe_2O_3 or its decomposition products, remain in LFP-C. This Mössbauer analysis suggests that the present carbothermal reduction and resulting $LiFePO_4$ generation have not been completed.

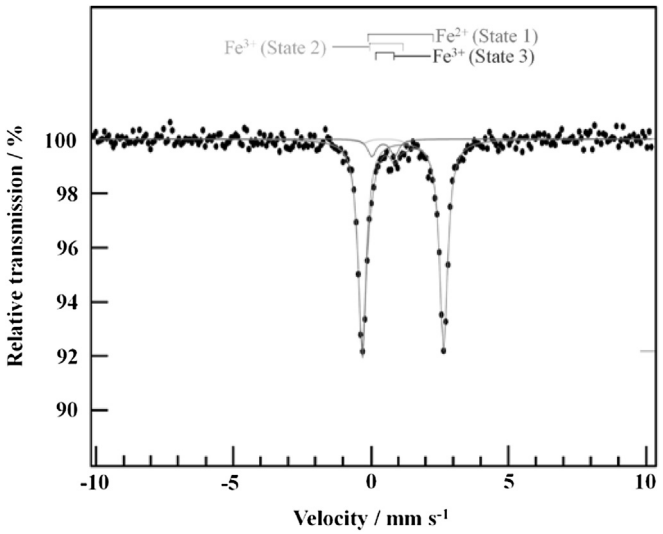

Fig. 4. Mössbauer spectrum of LFP-C.

Table 1
Summary of various parameters obtained by curve fitting of Mössbauer spectrum for LFP-C.

Component	Isomer shift δ/mm s^{-1}	Quadrupole splitting Δ/mm s^{-1}	Fe/%	Explanation
State 1	+1.23	2.96	91	Typical Fe^{2+}
State 2	+ 0.57	1.51	2	Low-symmetryFe^{3+}
State 3	+0.51	0.83	7	Fe^{3+}

Although synthesis of the $LiFePO_4$ phase is generally carried out under 700 °C [9,11,16] to avoid the generation of over-reduction byproducts, the rate-limiting step of $LiFePO_4$ phase generation in our method is probably carbothermal reduction because its reaction kinetics is very slow around 700 °C. Therefore, we raised the heating temperature to 900 °C to more quickly synthesize $LiFePO_4$/C without impurities. In this test, we only adopted citric acid as a carbon source. Fig. 5 shows the XRD patterns of the synthesized samples sintered at 900 °C for 120 s at 1500 °C min^{-1} (LFP-120) and for 90 s at 3000 °C min^{-1} (LFP-90). Since preliminary experiments showed that the reaction kinetics of the carbothermal reduction at 900 °C is extremely fast, we set the heating period very short at 900 °C. The olivine phase was confirmed in both LFP-90 and LFP-120, and their peak intensities exceeded LFP-C. From these results, we found that the crystallinity of synthesized samples significantly depends on the heating condition and the crystallinity is controllable. In addition, LFP-120 includes Fe_2P and Fe_3P, which are generated by the decomposition of $LiFePO_4$ due to an excessive reaction. Since we conclude that a 120-s heating period at 900 °C is too long to obtain $LiFePO_4$/C without impurities, we reduced the heating time to 90 s to limit the carbothermal reduction. We also applied a faster heating rate (3000 °C min^{-1}) since the carbothermal reduction starts around 700 °C and rapidly proceeds from 700 to 900 °C. The XRD pattern of LFP-90 shows a single $LiFePO_4$ phase, meaning that the generation of Fe_2P or Fe_3P is effectively suppressed. Although the lattice parameters of a $LiFePO_4$ phase in LFP-S and LFP-C (Fig. 1) cannot be determined because their peak intensities against the background are insufficient and the half

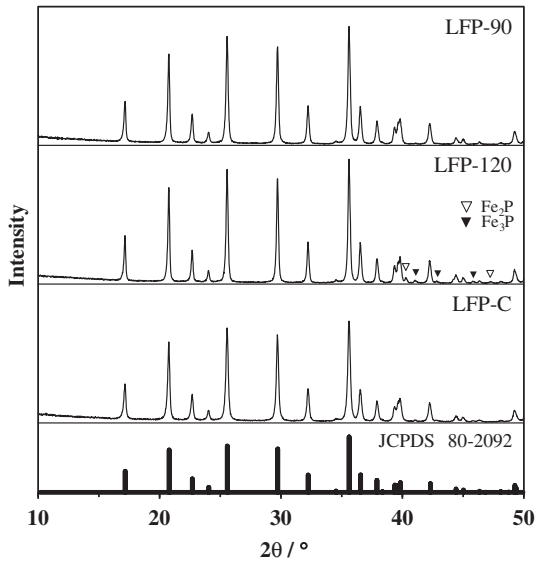

Fig. 5. XRD patterns of synthesized samples heated at 900 °C for 120 s (LFP-120) and 90 s (LFP-90). Profile of LFP-C (Fig. 1) is shown again for comparison of peak intensity. Reference pattern of $LiFePO_4$ phase (JCPDS 80-2092) is shown at the bottom.

peak-widths are too wide for reliable calculations, as seen in the comparison in Fig. 5, the LFP-90's lattes parameters can be refined and their values are $a = 10.321$ Å, $b = 6.011$ Å, and $c = 4.697$ Å, which are similar to the values reported in other studies [32–34].

Fig. 6 shows the SEM and TEM images of LFP-120 (a, b) and LFP-90 (c, d). LFP-120 contains secondary particles with diameters of submicron scale and a few micrometers (Fig. 6(a)), but LFP-90 only contains submicron particles (Fig. 6(c)). Since the 900 °C heating condition by high-frequency induction heating significantly increases the reaction and sintering rates, the secondary particle morphology varies in just 30 s. The TEM images show the morphology of the primary particles. The primary particle size of LFP-120 seems slightly larger than that of LFP-90 (Fig. 6(b) and (d)). The difference of just 30 s at 900 °C increases the primary particle size. Residual carbon, which was not consumed during the carbothermal reduction, exists on the $LiFePO_4$ surface. The carbon contents of these composites are estimated to be 2–3 wt.% from a series of our experiments and the amounts are the same or rather smaller when compared to other studies [10,13,21]. The carbon does not cover the entire surface; an exposed $LiFePO_4$ surface is observed in the TEM images. This result does not mean the inhomogeneous distribution of citric acid as a carbon source in the precursor. All of the $LiFePO_4$/C samples by heating at 900 °C become porous pellets, implying intense gas (CO_2, NH_3, or ethanol vapor) generation. The gases partially blew off the citric acid that covered the precursor, and thus the surface of the $LiFePO_4$ particles is partially exposed. If the exposed surfaces are making contact, the primary particle size will grow rapidly by sintering. Actually, however, the particle size growth was suppressed, which suggests that the porous shape formed by intense gas generation prevents contact between the $LiFePO_4$ particles. Intense gas generation might effectively suppress the particle size growth.

The primary particle size greatly affects the charge–discharge performances in $LiFePO_4$ with poor Li-ion conductivity. Fig. 7 shows the primary particle size distributions calculated by SAXS profiles. The average particle diameters of LFP-90 and LFP-120 are 54.5 and 72.8 nm, respectively. Although there is very little difference in the average particle size, LFP-120 contains some particles larger than 200 nm, and LFP-90 barely contains particles larger than 100 nm. The present primary particle size distributions reasonably correlate to the differences in the particle size observed in the above TEM images.

Fig. 8 shows the charge–discharge curves of the cathodes containing LFP-120 and LFP-90 at 1/10 and 10C-rates. A voltage plateau region based on a Fe^{2+}/Fe^{3+} redox couple extends more in both cathodes than in the LFP-C cathode. The LFP-120 and LFP-90 cathodes show discharge capacities of 136.7 and 153.3 mAh g^{-1} at the 1/10C-rate, and the LFP-90 cathode reaches 90% of the theoretical capacity. As a result of greatly improving the reaction kinetics of the carbothermal reduction by heating at 900 °C, the generation of the $LiFePO_4$ phase is completed within 120 s, which significantly improves the charge–discharge capacity. The lower discharge capacity of LFP-120 than LFP-90 can be attributed to the decreasing content of the $LiFePO_4$ phase in LFP-120 by the generation of the Fe_2P and Fe_3P phases. At the 10C-rate, the LFP-120 and LFP-90 cathodes show the discharge capacities of 74.1 and 100.1 mAh g^{-1}, and the voltage plateau remains flat.

Fig. 9 shows the charge–discharge rate performances of the LFP-120 and LFP-90 cathodes. As expected from the charge–discharge curves in Fig. 8, LFP-90's charge–discharge rate performance consistently exceeds LFP-120. Since Fe_2P with relatively good electrical conductivity acts as a conductive agent [31], it may improve the rate performance of LFP-120. However, LFP-120 has a crucial disadvantage of a relatively low Li-ion diffusion because its

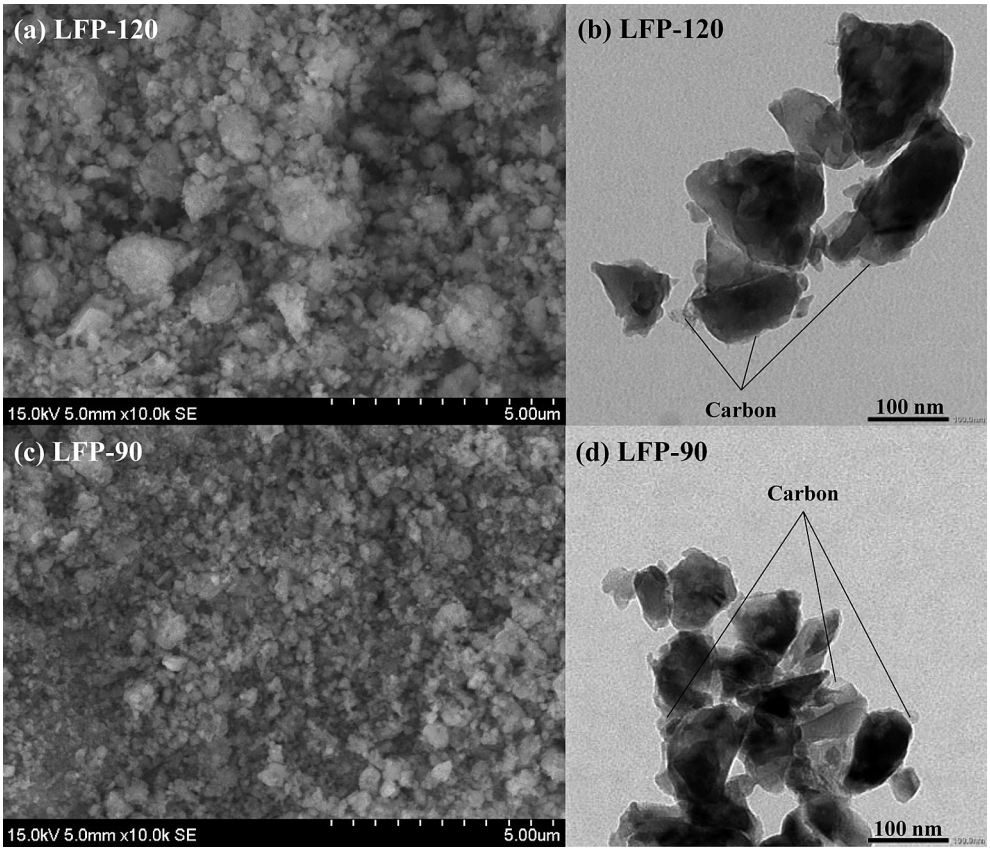

Fig. 6. SE images: (a) LFP-120, (c) LFP-90, and TEM images: (b) LFP-120, (d) LFP-90.

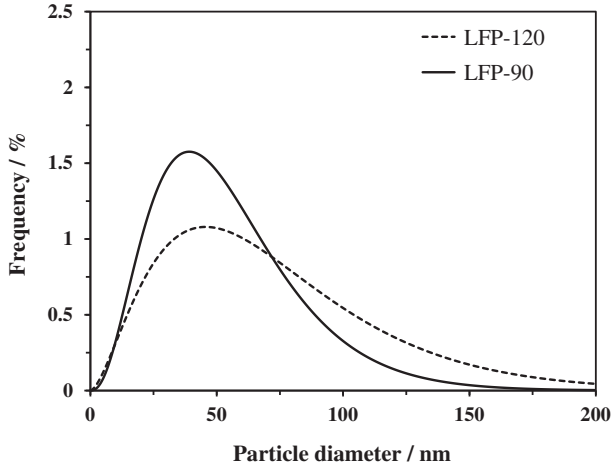

Fig. 7. Primary particle size distributions of LFP-120 and LFP-90 calculated from SAXS profiles.

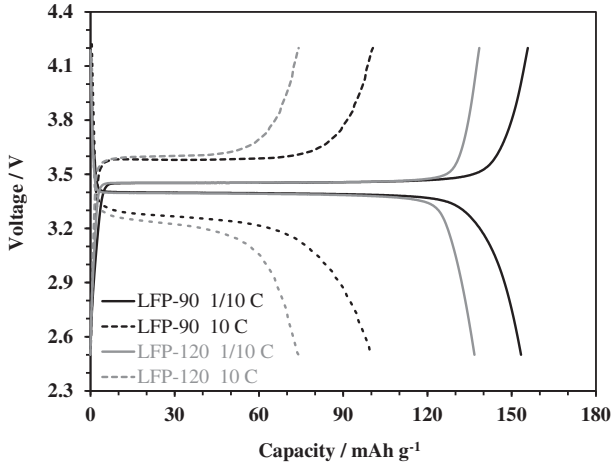

Fig. 8. Charge–discharge curves of cathodes containing LFP-120 and LFP-90 at 1/10 and 10C-rates (1C-rate = 170 mAh g^{-1}).

primary particle size is larger than that of LFP-90. Our present charge–discharge rate performance test also serves as a measure of cycle stability at high rates. Comparing the discharge capacity of the initial five cycles (1/10C-rate) with the last five cycles (1/10C-rate)

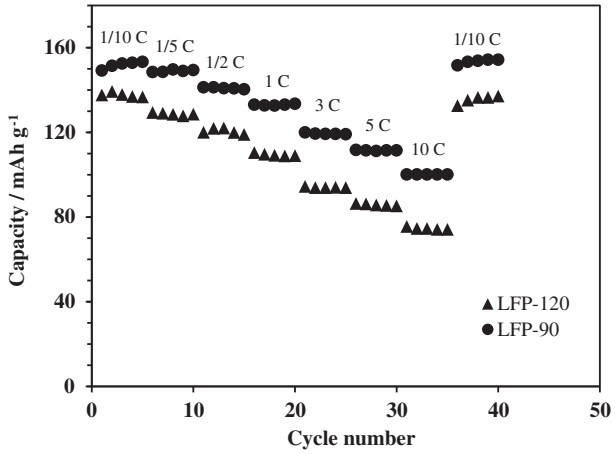

Fig. 9. Charge–discharge rate performance of cathodes containing LFP-120 and LFP-90 at various C-rates.

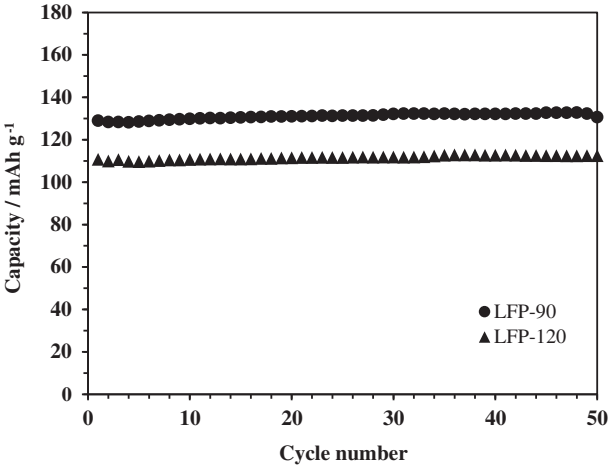

Fig. 10. Charge–discharge cycle performance of cathodes containing LFP-120 and LFP-90 at 1C-rate.

after various rate tests, their LFP-120 and LFP-90 values suggest no degradation. Furthermore, these composite materials show no degradation for 50 cycles at 1C-rate as shown in Fig. 10. LFP-120 and LFP-90 have excellent cycle stability inherent in $LiFePO_4$.

4. Conclusion

We successfully synthesized a $LiFePO_4$/C composite using Fe_2O_3 in far less time (within a few minutes) than the conventional method by combining carbothermal reduction with high-frequency induction heating. In our method, the carbon source is homogeneously dispersed, and citric acid is a suitable carbon source. LFP-C synthesized at 700 °C for 1 h contains a large amount of Fe^{3+} species derived from Fe_2O_3 because the carbothermal reduction is not completed. Consequently, the cathode containing LFP-C shows lower charge–discharge capacity (118.6 mAh g^{-1}) than theoretical capacity. Applying a higher heating temperature to improve the reaction kinetics increases the charge–discharge capacity by suppressing the residual Fe^{3+} species. The generation of such over-reduction byproducts as Fe_2P and Fe_3P can be suppressed by limiting the heating period. Although such heating time adjustments require accuracy in a range of seconds, the present high-frequency induction heating satisfies that request by its excellent controllability. LFP-90 synthesized in an optimized condition contains no impurities, and the particle size is sufficiently small to achieve desirable battery performances. The charge–discharge rate performance and the cycle stability of the cathode containing LFP-90 are excellent; the discharge capacity is 153.3 and 100.1 mAh g^{-1} at 1/10 and 10C-rates. In our method, since we obtained $LiFePO_4$/C with excellent battery performances in an extremely short period, we believe that this synthesis method can drastically reduce the cost of $LiFePO_4$/C cathode material and contribute to further applications of Li-ion batteries in various fields.

Acknowledgment

This work was partly supported by the “Strategic Project to Support the Formation of Research Bases at Private Universities”: a Matching Fund Subsidy from the Ministry of Education, Culture, Sports, Science and Technology (MEXT), 2009–2014.

References

[1] A.K. Padhi, K.S. Nanjundaswamy, J.B. Goodenough, J. Electrochem. Soc. 144 (1997) 1188.

[2] A.K. Padhi, K.S. Nanjundaswamy, C. Masquelier, S. Okada, J.B. Goodenough, J. Electrochem. Soc. 144 (1997) 1609.
[3] S.Y. Chung, Y.M. Chiang, Solid-State Lett. 6 (2003) A278.
[4] P.P. Prosini, M. Lisi, D. Zane, M. Pasquali, Solid State Ionics 148 (2002) 45.
[5] C. Delacourt, P. Poizot, S. Levasseur, C. Masquelier, Electrochem. Solid-State Lett. 9 (2006) A352.
[6] S. Ferrari, R.L. Lavall, D. Capsoni, E. Quartarone, A. Magistris, P. Mustarelli, P. Canton, J. Phys. Chem. C 114 (2010) 12598.
[7] P. Gibot, M. Casas-Cabanas, L. Laffont, S. Levasseur, P. Carlach, S. Hamelet, J.-M. Tarason, C. Masquelier, Nat. Mater. 7 (2008) 741.
[8] Y. Wang, Y. Wang, E. Hosono, K. Wang, H. Zhou, Angew. Chem. Int. Ed. 47 (2008) 7461.
[9] Z. Chen, J.R. Dahn, J. Electrochem. Soc. 149 (2002) A1184.
[10] H. Huang, S.C. Yin, L.F. Nazar, Electrochem. Solid-State Lett. 4 (2001) A170.
[11] A. Yamada, S.C. Chung, K. Hinokuma, J. Electrochem. Soc. 148 (2001) A224.
[12] D.H. Kim, J. Kim, Electrochem. Solid-State Lett. 9 (2006) A439.
[13] M. Koltypin, D. Aurbach, L. Nazar, B. Ellis, J. Power Sources 174 (2007) 1241.
[14] D. Choi, P.N. Kumta, J. Power Sources 163 (2007) 1064.
[15] K. Dokko, S. Koizumi, H. Nakano, K. Kanamura, J. Mater. Chem. 17 (2007) 4803.
[16] B. Ellis, W.H. Kan, W.R.M. Makahnouk, L.F. Nazar, J. Mater. Chem. 17 (2007) 3248.
[17] A.V. Murugan, T. Muraliganth, A. Manthiram, J. Phys. Chem. C 112 (2008) 14665.
[18] H. Yang, X. Wu, M. Cao, Yu. Guo, J. Phys. Chem. C 113 (2009) 3345.
[19] T. Muraliganth, A.V. Murugan, A. Manthiram, J. Mater. Chem. 18 (2008) 5661.
[20] M. Konarova, I. Taniguchi, Mater. Res. Bull. 43 (2008) 3305.
[21] M. Konarova, I. Taniguchi, J. Power Sources 194 (2009) 1029.
[22] J.K. Kim, G. Cheruvally, J.W. Choi, J.U. Kim, J.H. Ahn, G.B. Cho, K.W. Kim, H.J. Ahn, J. Power Sources 166 (2007) 211.
[23] G. Arnold, J. Garche, R. Hemmer, S. Strobele, C. Vogler, M.W. Mehrens, J. Power Sources 119–121 (2003) 247.
[24] M. Higuchi, K. Katayama, Y. Azuma, M. Yukawa, M. Suhara, J. Power Sources 119–121 (2003) 258.
[25] Y. Zhang, H. Feng, X. Wu, L. Wang, A. Zhang, T. Xia, H. Dong, M. Liu, Electrochim. Acta 54 (2009) 3206.
[26] L. Wang, Y. Huang, R. Jiang, D. Jia, Electrochim. Acta 52 (2007) 6778.
[27] J. Barker, M.Y. Saidi, J.L. Swoyer, Electrochem. Solid-State Lett. 6 (2003) A53.
[28] H.P. Liu, Z.X. Wang, X.H. Li, H.J. Guo, W.J. Peng, Y.H. Zhang, Q.Y. Hu, J. Power Sources 184 (2008) 469.
[29] Y. Lin, H. Pan, M. Gao, Y. Liu, J. Electrochem. Soc. 154 (2007) A1124.
[30] Y. Lin, M.X. Gao, D. Zhu, Y.F. Liu, H.G. Pan, J. Power Sources 184 (2008) 444.
[31] C.W. Kim, J.S. Park, K.S. Lee, J. Power Sources 163 (2006) 144.
[32] T. Nakamura, Y. Miwa, M. Tabuchi, Y. Yamada, J. Electrochem. Soc. 153 (2006) A1108.
[33] M.S. Islam, D.J. Driscoll, C.A.J. Fisher, P.R. Slater, Chem. Mater. 17 (2005) 5085.
[34] J.F. Martin, A. Yamada, G. Kobayashi, S. Nishimura, R. Kanno, D. Guyomard, N. Dupré, Electrochem. Solid-State Lett. 11 (2008) A12.